Cooperative behavior in periodically driven noisy integrate-fire models of neuronal dynamics

Adi R. Bulsara,[1,*] Tim. C. Elston,[2,†] Charles R. Doering,[2,‡] Steve B. Lowen,[3,§] and Katja Lindenberg,[4,‖]
[1]*Naval Command Control and Ocean Surveillance Center, Research, Development, Test, and Evaluation Division, Code 364, San Diego, California 92152-5000*
[2]*Center for Nonlinear Studies and Theoretical Division, MS-B258, Los Alamos National Laboratory, Los Alamos, New Mexico 87545*
[3]*Electrical Engineering Department, Columbia University, New York, New York 10027*
[4]*Department of Chemistry and Biochemistry B034, University of California at San Diego, La Jolla, California 92093-0340*
(Received 8 December 1995)

The dynamics of the standard integrate-fire model and a simpler model (that reproduces the important features of the integrate-fire model under certain conditions) of neural dynamics are studied in the presence of a deterministic external driving force, taken to be time-periodic, and white background noise. Both models possess resonant phenomena in the first passage probability distribution and mean first passage time, arising from the interplay of characteristic time scales in the system.

PACS number(s): 87.10.+e

I. INTRODUCTION

The response of nonlinear systems to weak periodic stimuli and noise has recently been of interest to the statistical physics community. One of the most intriguing cooperative effects that arises out of the coupling between deterministic and random dynamics in a nonlinear system is stochastic resonance (SR). This effect consists of a noise-induced enhancement in the signal-to-noise ratio measured at the frequency of the external driving force. The mechanism of SR is qualitatively easy to understand. Consider an overdamped particle moving in a potential with two local minima, or attractors. In the absence of external driving and noise, the particle will come to rest near one of the local minima. The effect of an applied periodic signal is then to rock the potential, alternately raising and lowering the local minima. If the amplitude of the signal is small compared to the height of the potential barrier separating the minima, the signal alone will not be able to induce switching events. In the presence of small amounts of noise, however, there will be a finite probability for the particle to escape over the potential barrier. Since the probability of escape is greater when the particle is in the "elevated" well, the noise-induced switching events may acquire some degree of coherence with the deterministic signal. With increasing noise, the ratio of the power spectral density to the background noise level at the frequency of the driving force increases, until for a critical noise strength the intrawell motion gives way to interwell (or hopping) motion as the major contributor to the dynamics. After this point the signal-to-noise ratio decreases with increasing noise strength, since the switching becomes noise-dominated and uncorrelated with the periodic signal. The optimal value of the noise strength occurs when the mean first passage time for interwell switching is close to half the modulation period. This matching of time scales is the reason for the characterization of this effect as a "resonance." Reviews of stochastic resonance and its potential applications to physics and biology can be found in recent review articles and conference proceedings [1] Related phenomena, first described by Doering and Gadoua [2] and known as "resonant activation," appear in randomly fluctuating barrier problems when the fluctuation time scale coincides with an escape time.

Recent work [3] has considered the possible role played by SR in the response of sensory neurons (modeled, for the most part, as noisy threshold devices) in the nervous system, and recent experiments [4] have indeed demonstrated SR-like behavior in sensory neurons. This has fueled speculation that SR may indeed play a role in signal processing by certain classes of neurons, and pointed to the need to quantify the phenomenon in simple mathematical models of neural firing that are not dynamical bistable systems.

Motivated by the above work, we consider one of the better-known models of neuron dynamics, the so-called "integrate-fire model." This model actually belongs to the class of continuous state space random walk models that embody some of the most fundamental concepts of statistical physics and can be applied to modeling phenomena in areas as diverse as genetics and astronomy. Good reviews of random walk dynamics [5] and classical theories of the first passage time in stationary one-dimensional random walks [6,7] can also be found in the literature.

The fundamental equation governing the integrate-fire model for neural dynamics is similar to an Ornstein-Uhlenbeck process with external driving:

$$\dot{x}=\lambda(u_r-x)+\mu+F(t)+A\cos\omega t. \tag{1}$$

Equation (1), in the absence of the periodic stimulus, has been extensively studied [8,9]. In these studies, $x(t)$ represents the cell membrane voltage, with μ being a positive drift to a firing threshold located at $x=a$, and λ being a decay constant governing the decay of the voltage back to a resting level u_r, taken to be zero for convenience throughout this work. The noise term $F(t)$ represents the net contribution

*Electronic address: bulsara@nosc.mil
†Electronic address: elston@cnls.lanl.gov
‡Electronic address: doering@cnls.lanl.gov
§Electronic address: steve6@ctr.columbia.edu
‖Electronic address: klindenberg@ucsd.edu

from all the synaptic inputs to the cell; it is usually taken to be Gaussian and δ correlated with zero mean and strength (or variance) $2D$. In this model the state variable $x(t)$ is assumed to make excursions to the firing threshold under the influence of the drift, noise, and signal. As soon as the threshold is reached, a firing event occurs and the neuron is reset deterministically to its starting point. The reset action renders the global dynamics nonlinear, with a represented mathematically as an absorbing barrier. Integrate-fire models provide convenient approximations to the full set of Hodgkins-Huxley equations used to describe neuronal behavior, under certain time-scale assumptions [10]. While the integrate-fire models do not provide complete descriptions of real neurons, they do capture many of their relevant properties. Integrate-fire models operate in two distinct regimes: (1) the deterministic firing regime and (2) the noise-activated regime. In the deterministic firing regime, the drift term μ in (1) is large enough so that firing events occur even in the absence of noise. The noise-activated regime corresponds to the case where the drift term alone is not sufficient to cause firing, and it is the noise that "kicks" the neuron across the firing threshold. A simplification of the above model, the so-called perfect integrator (corresponding to $\lambda=0$), constitutes the Gerstein-Mandelbrot [11] model. The interplay between noise and modulation in this simplified model was recently studied [12] at the level of the escape density function and the power spectral density of the spike train generated by barrier crossings. In the Gerstein-Mandelbrot description, the positive drift term μ represents the suitably weighted difference between excitatory and inhibitory synaptic inputs to the cell.

In Sec. II we construct an approximation to the first passage time probability density for the integrate-fire model. This is done through use of the Fokker-Planck equation for the probability density function $P(x,t)$ associated with (1), subject to the appropriate boundary conditions. The technique used to solve the Fokker-Planck equation is the method of images [7]. This method in general does *not* provide an exact solution for the (time-inhomogeneous) system (1), but subject to the appropriate caveats and constraints it provides approximate solutions that agree very well with results from numerical simulations of (1). More importantly, the noise-induced critical behavior that is the subject of this article is very accurately obtained via the method of images. We note that the system (1) may be recast in the form of the Ornstein-Uhlenbeck dynamics of a particle in the presence of a deterministically modulated absorbing boundary. In this form, this problem appears to have been first addressed, numerically, by Lansky [13]; we also point the reader to theoretical work [14] on random walks to moving barriers.

In Sec. III, we consider a simpler model for neural dynamics that is qualitatively similar to the integrate-fire model. This model consists of an overdamped particle subjected to a constant force, periodic driving, and noise. One advantage of this model is that in the absence of periodic driving, solutions of the Fokker-Planck equation governing this process have a relatively simple analytic form. An exact solution to the level crossing problem for the Ornstein-Uhlenbeck process with $A=0$ exists [6,15], but the incorporation of the periodic driving ($A>0$) dictates that we adopt the more tractable approach. The solution to the simpler model is expressed in terms of eigenfunctions of the Fokker-Planck operator, and using perturbation techniques we are then able to construct an asymptotic solution for the case of weak-amplitude, low-frequency periodic forcing. Note that this "linear ramp" approximation could be applied in both deterministic firing and noise-activated regimes; however, we apply it only to the noise-activated regime in this work. This is because the images technique, applied to the exact integrate-fire model, yields good agreement with simulations in the subthreshold (or deterministic firing) regime, for the signal parameters considered in this work; in this regime the dynamics (1) are drift-dominated. We reiterate, however, that the method of images yields the correct qualitative behavior, including the cooperative interaction between the signal and noise, even in the noise-activated regime.

Sections IV and V are devoted to discussions of the results and limitations of our theories. In Sec. IV the important properties of the first passage time probability density for both models are elucidated, and in Sec. V the resonant behavior exhibited by these systems is explained. This behavior is in line with recent treatments of SR [12,16] that define the resonance as a matching between the modulation period and the location of the maxima in the first passage time probability density, and effectively links SR to a synchronization phenomenon.

It is important to note that periodic modulations of the type considered here are seldom encountered in real neurons, possible exceptions being in auditory, olfactory, and some other classes of sensory neurons. In this vein, we mention that SR (characterized via the occurrence of a maximum in an output signal-to-noise ratio) has been demonstrated recently [17] in integrate-fire models of the form (1), subject to time-periodic spike trains embedded in Poisson noise. Our treatment does, however, provide a stepping stone to the modeling of the response to more complex signals and also provides an explanation, based on well-accepted models of neural dynamics, of cooperative behavior that has been observed in recent experiments.

II. PERIODICALLY DRIVEN INTEGRATE-FIRE MODEL

The integrate-fire system models the firing process via the dynamics (1) and may be visualized as an overdamped particle subjected to the potential

$$U(x)=\frac{\lambda}{2}x^2-\mu x \tag{2}$$

that has a minimum at $c=\mu/\lambda>0$. A firing event occurs when the particle reaches the absorbing barrier: following each firing, the potential is reset, deterministically, to the same starting point. This situation is depicted in Fig. 1. For a starting point $x_0<c$, the model admits deterministic firing, i.e., firing induced solely by the positive drift, when the barrier is located to the left of the minimum, or equivalently, when $a\lambda/\mu<1$. For $A=0=F(t)$, one readily verifies that the time taken to reach the barrier at $x=a$ starting from $x=0$ is

$$t_{a0}=-\lambda^{-1}\ln\left(1-\frac{a\lambda}{\mu}\right). \tag{3}$$

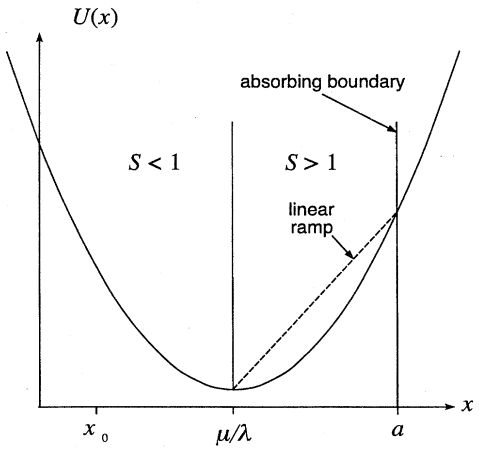

FIG. 1. Parabolic potential "felt" by the "particle." $x=a$ is the location of the absorbing barrier. The dashed line is the approximation to the potential used in the linear ramp model, and the area enclosed between it and the parabola determines the validity of this approximation.

For $0<A\ll\mu$, $\omega\ll\mu/A$, and $\omega\ll\lambda$ an approximation to the deterministic passage time is

$$t_a \approx -\lambda^{-1} \ln\left[\frac{1-\frac{a\lambda}{\mu}+\frac{A\lambda^2/\mu}{\lambda^2+\omega^2}}{1+\frac{A\lambda^2/\mu}{\lambda^2+\omega^2}}\right]. \tag{4}$$

Note that the conditions on the frequency ω constitute an adiabatic approximation that assumes a separation of time scales between the external forcing period and other times intrinsic to the system. In what follows, we will frequently refer to the $a\lambda/\mu<1$ regime as the deterministic firing regime and $a\lambda/\mu>1$ as the noise-activated regime.

Throughout this work, we assume the noise to be white, with zero mean:

$$\langle F(t)\rangle=0, \quad \langle F(t)F(s)\rangle=2D\delta(t-s).$$

The Fokker-Planck equation for the time-dependent probability density for the process (1) is [18]

$$\frac{\partial P}{\partial t}=-\frac{\partial}{\partial x}(\mu+A\cos\omega t-\lambda x)P+D\frac{\partial^2 P}{\partial x^2}. \tag{5}$$

The "free" solution to (5) [i.e., boundaries at $\pm\infty$ and $P(x,t=0)=\delta(x-x_0)$] was originally found by Uhlenbeck and Ornstein [8], and is

$$P(x,t)=\frac{1}{\sqrt{2\pi\alpha(t)}}\exp\left[-\frac{[x-\beta(t)]^2}{2\alpha(t)}\right], \tag{6}$$

where

$$\alpha(t)=\frac{D}{\lambda}(1-e^{-2\lambda t}), \tag{7}$$

$$\beta(t)=x_0e^{-\lambda t}+\frac{\mu}{\lambda}(1-e^{-\lambda t})+\frac{A}{\lambda^2+\omega^2}(\lambda\cos\omega t+\omega\sin\omega t-\lambda e^{-\lambda t}). \tag{8}$$

To construct an approximate solution $P_a(x,t)$ that incorporates an absorbing boundary at $x=a$, an "image particle" is placed at $x=2a-x_0$. The solution P_a is the superposition of the free solutions for the particle and its image, i.e.,

$$P_a(x,t)=P(x,x_0,t)+QP(x,2a-x_0,t), \tag{9}$$

where Q is found by requiring that (9) solves the Fokker-Planck equation (5) with the specified boundary conditions. Setting $P_a(x=a,x_0,t)=0$ yields

$$Q=-e^{\psi(t)}, \tag{10}$$

where

$$\psi(t)=\frac{2}{\alpha(t)}(x_0-a)[a-\beta(t)-ae^{-\lambda t}]e^{-\lambda t}. \tag{11}$$

The solution of (5) that incorporates the boundary at $x=a$ is

$$P_a(x,t)=\frac{1}{\sqrt{2\pi\alpha}}\left[\exp\left(-\frac{[x-x_0e^{-\lambda t}-\beta(t)]^2}{2\alpha}\right)-e^{\psi(t)}\exp\left(-\frac{[x-(2a-x_0)e^{-\lambda t}-\beta(t)]^2}{2\alpha}\right)\right], \tag{12}$$

provided $\dot{\psi}=0$. This restriction requires that

$$\lambda[a-\beta(t)-ae^{-\lambda t}]+\dot{\beta}(t)-a\lambda e^{-\lambda t}=0. \tag{13}$$

For the case of no modulation ($A=0$), the condition (13) reduces to

$$S\equiv\frac{a\lambda}{\mu}=0 \text{ or } 1. \tag{14}$$

Thus, the method of images produces an exact result (for $A=0$) when (1) $\lambda=0$ (corresponding to the Gerstein-Mandelbrot model, or (2) the firing threshold is located at the minimum of the potential. The case of nonzero modulation is somewhat trickier. Using the definition (13) we find that the method of images will yield good results when $A\ll\mu$, and ω is the slowest frequency in the system. In the remainder of this work, when we use the method of images and consider the firing dynamics above the deterministic threshold, we will assume that the firing threshold is located close to the deterministic firing threshold $S=1$. We will show that even a deliberate violation of the above conditions for the validity of the method of images (done in order to better elucidate the cooperative behavior that is the subject of this article) still leads to extremely good agreement with numerical simulations.

Once $P_a(x,t;x_0,0)$ is known, the first passage time probability density can be calculated via the well-known prescription

$$g(t)=-\frac{d}{dt}\int_{-\infty}^{a}P_a(x,t;x_0,0)dx. \tag{15}$$

For the probability distribution (12),

$$g(t)=\frac{2(a-x_0)e^{-\lambda t}}{\sqrt{2\pi\alpha^3}}\left(\lambda\alpha+\frac{\dot{\alpha}}{2}\right)e^{-w^2}+\frac{\dot{\psi}}{2}e^{\psi}[1+\Phi(z)], \tag{16}$$

where

$$z=\frac{a-(2a-x_0)e^{-\lambda t}-\beta(t)}{\sqrt{2\alpha}},$$

$$w=\frac{a-x_0e^{-\lambda t}-\beta(t)}{2\alpha},$$

and

$$\Phi(z)=\frac{2}{\sqrt{\pi}}\int_0^z e^{-y^2}dy$$

is the error function. Setting $\lambda=0$ yields the "perfect integrator" results [12], and setting $A=0$ and $S=1$ yields an exactly solvable case [9,19]:

$$g_0(t)=\frac{2D(a-x_0)e^{-\lambda t}}{\sqrt{2\pi\alpha^3}}\exp\left[-\frac{(ae^{-\lambda t}-x_0)^2}{2\alpha}\right]. \tag{17}$$

We will mainly be concerned with the noise-activated regime, $S>1$. For this regime, the method of images is not exact even for $A=0$.

III. LINEAR RAMP MODEL

As motivation for this model, we consider the noise-activated regime and, via the translation $y=x-c$, write the equation of motion for the process in the form

$$\dot{y}=-\lambda y+F(t), \tag{18}$$

where the potential function is

$$U(y)=\frac{\lambda}{2}y^2-\frac{\mu^2}{2\lambda} \tag{19}$$

with the firing threshold (absorbing barrier) located at $L=a-c$. First consider the $A=0$ case. The firing time for the neuron may be viewed as arising from two distinct events. The first event is the drift-dominated passage to the minimum of the potential located at $y=0$, and the second corresponds to the passage from the potential minimum to the absorbing barrier at $y=L$. We assume that once the particle crosses the minimum from its starting position at $y=y_0$, it will never recross the minimum in the opposite direction, i.e., we assume a "one-way" barrier at $y=0$. Past this barrier, i.e., for $0<y\leq L$, the dynamics are noise dominated, and we take t_1 to be the passage time corresponding to a particle trapped between a reflecting barrier at $y=0$ and an absorbing barrier at $y=L$. We further assume that in this region the potential can be replaced by a straight line, or ramp connecting the points $y=0$ and $y=L$:

$$U(y)=\frac{\lambda L}{2}y-\frac{\mu^2}{2\lambda} \tag{20}$$

with the equation of motion ($h\equiv\lambda L/2$),

$$\dot{y}=-h+F(t). \tag{21}$$

It is readily apparent that we have effectively replaced the exact dynamics, in the noise-dominated regime, by an equivalent dynamics that have the form of the perfect integrator model [11,9,12].

To compute the probability density for t_1, the Fokker-Planck equation

$$\frac{\partial P}{\partial t}=h\frac{\partial P}{\partial y}+D\frac{\partial^2 P}{\partial y^2} \tag{22}$$

is solved subject to the absorbing boundary at $y=L$,

$$P(y=L,t)=0 \tag{23}$$

and the reflecting boundary condition at $y=0$,

$$\left(h+D\frac{\partial}{\partial y}\right)P(y,t)|_{y=0}=0. \tag{24}$$

The solution is derived using the standard separation of variables technique; we assume solutions of the form $P(y,t)=e^{-\lambda_n t}q_n(y)$. The eigenfunctions q_n have the general form

$$q_n=C_1e^{k_n^+ y}+C_2e^{k_n^- y}, \tag{25}$$

and the $k_n^{\pm}$ are related to the eigenvalues λ_n by

$$k_n^{\pm}=-\frac{h}{2D}\pm\frac{1}{2}\sqrt{\left(\frac{h}{D}\right)^2-\frac{4\lambda_n}{D}}. \tag{26}$$

For convenience the eigenfunctions are written in the form

$$q_n(y)=e^{-h/2Dy}b_n(y). \tag{27}$$

For $n>1$, b_n has the form

$$b_n=\sin k_n(y-L) \tag{28}$$

and k_n must be determined from the characteristic equation

$$\tan k_nL=\zeta k_nL, \tag{29}$$

where $\zeta=2D/hL$. The eigenvalues are determined by the relation

$$\lambda_n=\frac{h^2}{4D}+Dk_n^2. \tag{30}$$

The functional form of b_1 is determined by the value of ζ. If $\zeta>1$ then b_1 is given by (28) and k_1 and λ_1 satisfy Eqs. (29) and (30), respectively. If $\zeta=1$ then $b_1=1-y/L$, $k_1=0$, and $\lambda_1=h^2/4D$. If $\zeta<1$ then $b_1=\sinh k_1(y-L)$, $\tanh k_1L=\zeta k_1L$, and $\lambda_1=h^2/4D-Dk_1^2$.

The general solution to (22) is then written as the expansion

$$P(y,t|y_0,0)=e^{-hy/2D}\sum_n C_n e^{-\lambda_n t}b_n(y) \tag{31}$$

with the constants C_n determined from the initial condition $P_n(y,0|y_0,0)=\delta(y-y_0)$:

$$C_n=\frac{e^{hy_0/2D}b_n(y_0)}{\int_0^L b_n^2(y)dy}. \tag{32}$$

For $n>1$, C_n has the form

$$C_n=\frac{e^{hy_0/2D}\sin[k_n(L-y_0)]}{\frac{L}{2}-\frac{\sin 2k_nL}{4k_n}}. \tag{33}$$

If $\zeta<1$ then C_1 is given by (33); if $\zeta>1$ then

$$C_1=-\frac{e^{hy_0/2D}\sinh[k_1(L-y_0)]}{\frac{L}{2}-\frac{\sinh 2k_1L}{4k_1}}. \tag{34}$$

There is nothing special about the $\zeta=1$ case, so for convenience it will not be considered.

Using (15), the first passage time probability density for this process is found to be

$$g_1(t)=-D\frac{\partial}{\partial y}P(y,t|0,0)|_{y=L} \tag{35}$$

$$=De^{-hL/2D}\sum_n \frac{k_nb_n(0)e^{-\lambda_n t}}{\int_0^L b_n^2(y)dy}, \tag{36}$$

where we set $y_0=0$, since the starting point is always the minimum of the potential (19). Finally, we obtain the approximate first passage time probability density for the entire firing process as the convolution:

$$g(t)=\int_0^t g_0(r)g_1(t-r)dr, \tag{37}$$

where $g_0(r)$ is the probability density for the reset time. If the average reset time is short compared with the escape time, then $g(t)$ will have the same form as $g_1(t)$ and be only shifted slightly toward later times. In this description, we are tacitly identifying the drift-dominated passage to the minimum of the potential with a "reset." For simplicity, we shall take $g_0=\delta(0)$, corresponding to an instantaneous reset. A finite reset time can be incorporated into this model in a variety of ways, e.g., by using the (exact) density function (17) for $g_0(t)$, or by assuming an exponentially distributed reset, $g_0(t)=\tau^{-1}e^{-t/\tau}$, where τ is a fitting parameter. For the case of the noninstantaneous reset, the mean reset time may be obtained through a computation of the first moment of the density function $g_0(t)$. The case of a noninstantaneous reset will be treated briefly, for the $A=0$ case, in the following section and in greater detail in a future publication.

When periodic forcing is included in the dynamics, the Fokker-Planck equation for the simplified model is

$$\frac{\partial P}{\partial t}=(h-A\sin\omega t)\frac{\partial P}{\partial y}+D\frac{\partial^2 P}{\partial y^2} \tag{38}$$

with the boundary conditions $P(L,t)=0$, and $[h-A\sin\omega t+D(\partial/\partial y)]P(y,t)|_{y=0}=0$. Note that we will use for convenience, throughout our treatment of the linear ramp approximation, an $A\sin\omega t$ driving term, in contrast to the treatment of the preceding section. Equation (38) does not admit an exact analytic solution. However, it is easy to verify, by direct substitution into (38), that a solution correct up to first order in A and ω is

$$P(y,t|y,0)\approx e^{-(h-A\sin\omega t)y/2D}\sum_n C_n e^{\int_0^t\lambda'(s)ds} \times\sin[k_n'(L-y)], \tag{39}$$

where

$$k_n'=\frac{h-A\sin\omega t}{2D}\tan k_n'L \tag{40}$$

and

$$\lambda_n'=\frac{(h-A\sin\omega t)^2}{4D}+Dk_n'^2. \tag{41}$$

In general if $\zeta<1$, then for the first term in (39) the tangent in (40) would become a hyperbolic tangent. For the cases we study in Secs. IV and V, when $\zeta<1$ the small values of the noise strength D invalidate the approximate solution (39). Therefore, for the rest of this section we restrict ourselves to case $\zeta>1$. Letting $k_n'=k_n+A\delta_n\sin\omega t$ and $\lambda_n'=\lambda_n+A\gamma_n\sin\omega t$ and using (40) and (41), we can write the approximate conditional probability density given by (39) in the form

$$P(y,t|y_0,0)\approx e^{-(h-A\sin\omega t)y/2D}\sum_n C_n e^{-\lambda_n t-A\gamma_n/\omega[1-\cos(\omega t)]} \times\sin[(k_n-A\delta_n\sin\omega t)(L-y)], \tag{42}$$

where

$$\delta_n=\frac{\tan k_nL}{2D\left(1-\frac{hL}{2D}\sec^2 k_nL\right)},$$

and $\gamma_n=2D\delta_n-h/2D$. Using (36) and keeping terms only to first order in ω and A, we obtain an approximation to the first passage time probability density,

$$g_1(t)\approx e^{-hL/2D}\sum_n C_n e^{-\lambda_n t-A\gamma_n(1-\cos\omega t)/\omega} \times\left[k_n-A\left(\delta_n-k_n\frac{h}{2D}\right)\sin\omega t\right]. \tag{43}$$

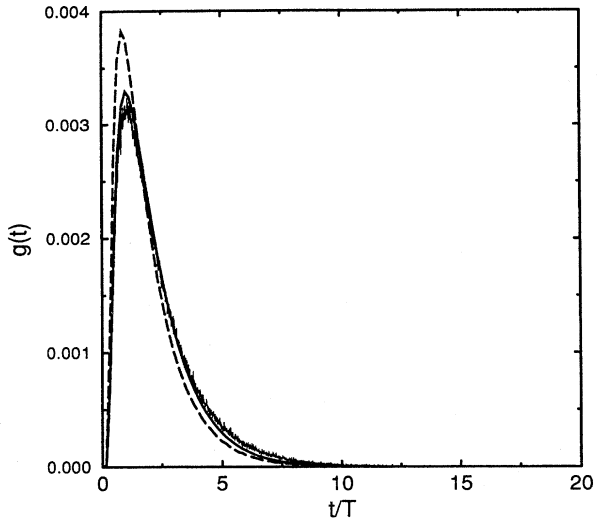

FIG. 2. First passage time probability density for $A=0$ computed via numerical simulation of (1), method of images result (16) (solid curve), and eigenfunction expansion (40) (dashed curve). $a=20$, $\mu=0.11$, $\lambda=0.006$, $D=0.5$, $R=0.001$, $\zeta=119.5$. The horizontal scale is normalized to the period $T=2\pi/\omega$, where $\omega=0.05$.

IV. PROPERTIES OF THE FIRST PASSAGE TIME DENSITY FOR $A=0$

In this section we study the properties of the first passage time probability density in the absence of external driving. The method of images yields an accurate approximation to the probability density below the deterministic switching threshold (i.e., for $S<1$), the motion in this regime being drift-dominated. Of course, for $\lambda=0$ or $S=1$ the method of images yields the exact behavior. For the noise-activated case the method of images yields good qualitative agreement when the absorbing barrier is not too far from the minimum of the potential; the agreement improves with increasing noise strength and/or drift. In theory, (36) is the exact first passage time probability density for the linear ramp model (past the potential minimum). In practice, however, the distribution must be approximated by keeping a finite number of terms in the infinite series. A comparison (not shown) with numerical simulations reveals that keeping as few as two terms in the summation produces an excellent approximation to the distribution.

In Fig. 2 we plot the first passage density obtained via direct simulation of (1), together with the method-of-images result (16). In this figure $S=1.1$, and we expect the images result to agree well with the numerically obtained probability density. Indeed it does agree, and this agreement is further improved by increasing the noise strength. In this figure we also show the density function (37) obtained using the linear ramp model with the reset interval density function given by the (exact) expression (17). Note that the position of the mode of the distribution is correctly captured by the method of images and the ramp model.

It is possible to quantify the conditions under which the linear ramp model provides a good approximation to the dynamics past the potential minimum. Two parameters determine the agreement of the linear ramp model with the method of images results: the parameter $\zeta\equiv 2D/hL$ which was defined in the context of the eigenvalue equation (29), and the ratio $R\equiv(\lambda L^3/12)/L$, which is seen as the ratio of the area of the sector enclosed by the potential (19) and the straight line (20) (refer to Fig. 1), to the distance of the absorbing barrier from the minimum of the potential (19). The best agreement between the linear ramp model and numerical results is obtained for $R\ll 1$ and $\zeta\gg 1$. We observe that, for fixed a,μ,λ, increasing the noise variance $2D$ leads to an increase in ζ so that in general the best agreement is obtained in the noise-dominated regime; this is also the regime where we look for the interesting noise-induced cooperative behavior, e.g., stochastic resonance. The series in (36) converges more rapidly with increasing ζ; even for regimes far above the threshold, i.e., $S\gg 1$, good agreement can still obtained by increasing the noise variance.

When considering the firing behavior in the absence of modulation, the two time scales of interest are the mean first passage time t_0 and the mode (maximum value) t_m of the probability density. Both these quantities are functions of the noise, drift, and barrier height. Depending on the values of these parameters the mean can be close to the mode, corresponding to a Gaussian-like density, or the mean can be far out in the tail of the distribution. For the linear ramp model (assuming an instantaneous reset) the mean and mode are well approximated by the following expressions:

$$t_0=De^{-hL/2D}\left[\frac{C_1k_1}{\lambda_1^2}+\frac{C_2k_2}{\lambda_2^2}\right] \tag{44}$$

and

$$t_m=\frac{1}{\lambda_2-\lambda_1}\ln\left[-\frac{C_2k_2\lambda_2}{C_1k_1\lambda_1}\right]. \tag{45}$$

These expressions come from keeping the first two terms of the summation in (36), and produce visually indistinguishable results when compared against the mean and the mode calculated using the first 21 terms in (36) (data not shown).

For the leaky integrate-fire model in the deterministic firing regime ($S<1$) the mean value t_0 approaches the constant value a/μ in the $\lambda\to 0$ limit. This is the well-known mean value for the Wiener process. In the $D\to 0$ limit, the mean first passage time approaches (for $\lambda>0$) the deterministic value t_{a0}. Above threshold, t_0 is strongly noise-dependent. The mode is (for any S) *always* a function of the noise and may be the more important of the two measurements, particularly for the highly skewed first passage densities of certain neural dynamics [9]. In experiments in which finite amounts of data are available, firing events clustered about the mode are more probable. For very low noise, the distribution is sharply peaked with a very short tail, and in this limit, the mean and the mode approach one another. Virtually identical results are obtained for increasing drift with the important difference that, as μ increases, the mode and the mean shift to lower values. This is not surprising; the passage times to the barrier become shorter (corresponding to increasing firing rates) with increasing drift. The large μ limit yields results that increasingly approach the Wiener process results, since the λ dependence becomes weaker and weaker. In the limit $D\to 0$, or $\mu\to\infty$, the distribution col-

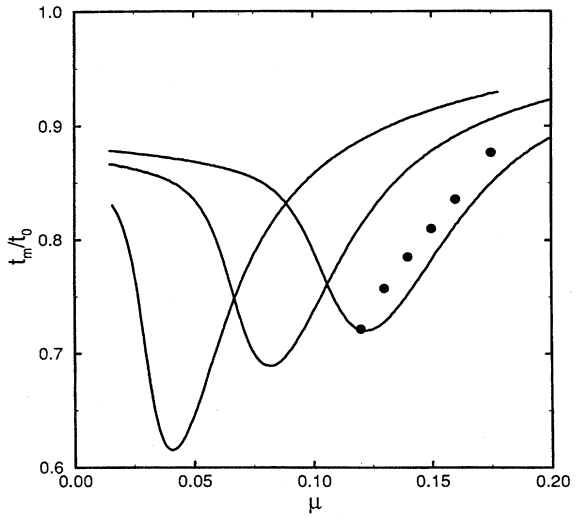

FIG. 3. Mode-to-mean ratio (computed via method of images) vs drift coefficient μ for $A=0$ and $a=20$, $D=0.075$, and $\lambda=0.002$, 0.004, 0.006 (reading from left to right). Minima of the curves correspond to the deterministic switching threshold, $S=1$. Data points correspond to simulation results (deterministic firing regime) for $\lambda=0.006$ case.

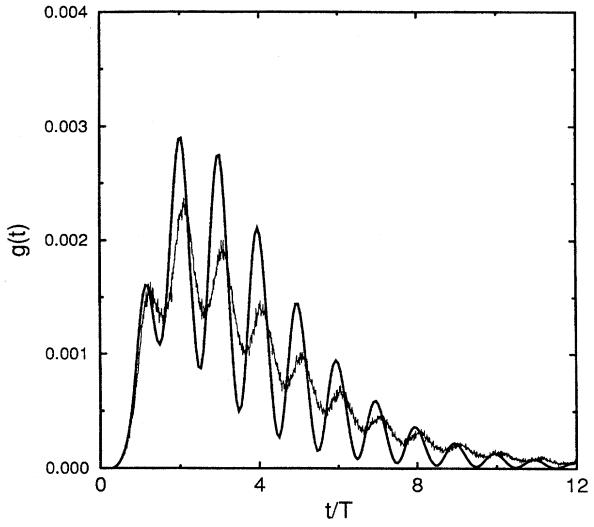

FIG. 4. First passage time density obtained via method of images, Eq. (16) (smooth curve) and numerical simulation of (1) (jagged curve). $a=30$, $\mu=0.11$, $\lambda=0.004\,14$, $A=0.035$, $\omega=0.05$, $D=0.5$; noise-activated case, $S=1.13$.

lapses into a single δ-like peak. In this limit t_0 approaches the deterministic value given by (3).

Figure 3 shows the ratio t_m/t_0 (computed using the method of images) versus μ for different values of the decay constant λ. The minima of the curves correspond to the deterministic crossing threshold for each case. Past this threshold, i.e., for decreasing μ, the ratio S decreases until for large drifts, the process becomes drift-dominated and the probability density is once again sharply peaked; in this regime $t_m/t_0 \to 1$. The opposite limit ($\mu \to 0$) is not shown in this figure. This limit, corresponding to extremely large values of S, covers the regime of near-exponential behavior in the first passage density function; the crossings are uncorrelated and the process is renewal, with very long mean first passage times ($t_0 \gg \lambda^{-1}$). We do not consider this limit in this paper. For the $\lambda=0.006$ case, we show data points corresponding to a computation of the ratio t_m/t_0 from numerical simulations, in the deterministic firing regime where the method of images is expected to yield the correct qualitative behavior. In the noise-activated regime, numerical simulations tend to run too slowly (due to the smaller values of μ) to yield this ratio with the desired accuracy.

V. PERIODIC DRIVING AND RESONANCE BEHAVIOR

Consider the first passage time probability density for the $A>0$ case. For both models, at very low stimulus frequencies ($\omega \ll 2\pi/t_m$) the distribution consists of a single peak located at $t=t_m$, and the dynamics are dominated by the drift and the noise. Increasing the frequency ω leads to the development of additional peaks in the distribution, their precise position depending on the initial phase of the driving force. For small amplitude driving, the overall shape of distribution is still largely determined by the $A=0$ case. In particular the location of the mode is preserved. Figures 4–6 show the first passage time probability density for the integrate-fire model with $A>0$, and Fig. 7 is for the linear ramp approximation. In all these figures, the smooth curve is the analytic approximation to the distribution and the jagged curve is derived from numerical simulations of (1) and (21). Note that, in Figs. 4–6, we have deliberately used a higher value A of the signal amplitude than is allowed by the constraints associated with the method of images; this has been done to elucidate the peak structure in the presence of finite A. One observes that the analytic approximation yields taller peaks than the numerics; however, the locations of these peaks (at $t=nT\equiv 2n\pi/\omega$) and their relative heights agree well with numerical results even in regimes where one expects the ap-

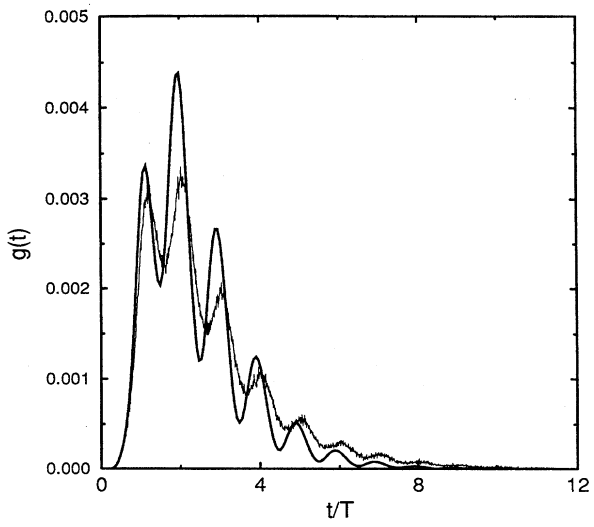

FIG. 5. Same as Fig. 4 except $\mu=0.2$, $\lambda=0.007\,53$; $S=1.13$.

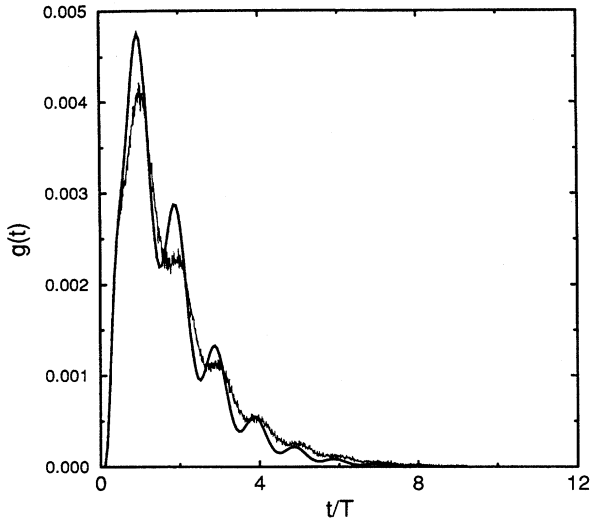

FIG. 6. Same as Fig. 4 except $\mu=0.2$, $\lambda=0.007\,53$, $D=1.5$; $S=1.13$.

proximations of Sec. II to break down. We shall see, in fact, that the interesting resonance behavior of the peak heights and the mean first passage time is closely predicted by the method of images even for these large A values. We readily observe that increasing μ leads to a shrinking of the tail of the distribution and a greater concentration of probability in the low-lying peaks. The motion tends to be increasingly drift-dominated (as μ is increased) with the mean first passage time decreasing. As μ is increased still further, one obtains a distribution in which most of the probability is in the $n=1$ peak with very small outlying peaks. An analogous effect is seen in Fig. 6 when we hold μ constant and increase the noise strength D. Increasing the noise strength further shrinks the tail of the density function (leading to a corresponding decrease in the mean first passage time) with the $n=1$ peak growing at the expense of the remaining peaks. The maximum of the $n=1$ peak as a function of noise has been related to stochastic resonance in bistable systems [16]. We expand upon these ideas below. Note that increasing the drift and/or noise, or decreasing the barrier height while keeping the ratio S fixed, leads to better accuracy in the images-based approximation. As already noted, the approximation produces the correct qualitative behavior beyond its region of validity.

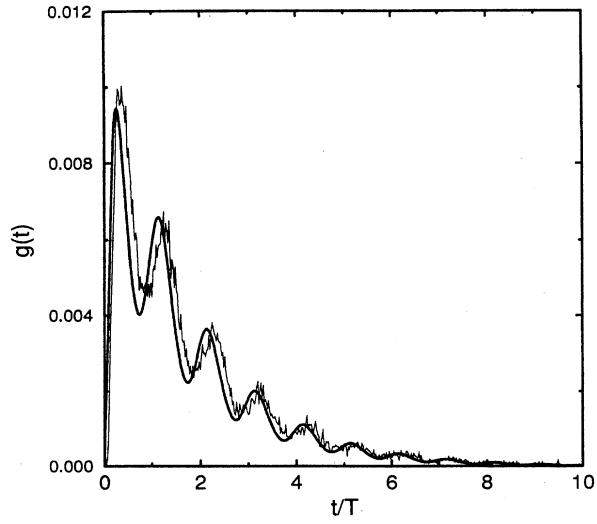

FIG. 7. First passage time density for the linear ramp model (instantaneous reset). Jagged curve: numerical simulations of (21) with $A\sin\omega t$ driving; smooth curve: perturbation result (five terms) (51). $a=9.0$, $h=0.1$, $D=0.6$, $\omega=0.1$, and $A=0.03$.

Note that Figs. 4–7 were produced with $S>1$, that is, the firing events are noise activated. In the deterministic firing regime ($S<1$), the dynamics tends to be drift-dominated with the probability concentrated in the first few peaks of the distribution. This regime is a superset of the perfect integrator for which the method of images produces the correct qualitative behavior [12]. The critical ($S=1$) case also admits good agreement between the method-of-images approximation and the numerically obtained result. In all cases, but particularly below the deterministic firing threshold (i.e., for $S\leq 1$) the mean and mode are very accurately predicted by the images-based approximation.

The linear ramp model displays the same qualitative features as the integrate-fire model. The first passage time density for this model is shown in Fig. 7. The parameter values used to generate this figure were $A=0.03$, $\omega=0.05$, $h=0.1$, and $D=0.6$, and as can be seen for these values there is good agreement between the approximate analytic expression for the density and the numerical simulations. Similar to the integrate-fire model, the relative peak heights are functions of both the drive frequency and noise amplitude.

It is important to point out that, for the range of signal amplitudes used in this work, the agreement between the three approaches (numerical integration of the stochastic differential equation, method of images and linear ramp model) for $A>0$ is determined by the agreement for $A=0$. For $A>0$, the density function is the $A=0$ density with peaks superimposed at the appropriate locations. While the perturbation theory may lead to small vertical differences in the peak heights, as described earlier, the degree of agreement between the results derived from the three approaches for $A>0$ will depend primarily on what is seen in Fig. 2 for $A=0$.

Now consider the heights of individual peaks as functions of the noise strength and the modulation frequency. In Fig. 8 we show the heights of individual peaks of the density function (16) as a function of the noise strength D; the discrete points are obtained from numerical simulations of (1). The peaks are seen to go through maxima at critical D values. Similar behavior is observed in the deterministic firing regime. Equation (16) can be used to compute the critical values of D via simple differentiation and by noting that the nth peak is located at $t=nT$. After some calculation, we find

$$D_{nc}\approx\frac{\mu^2/\lambda}{1-e^{-2n\lambda T}}\left[e^{-n\lambda T}-\left(1-\frac{a\lambda}{\mu}+\frac{A\lambda^2/\mu}{\lambda^2+\omega^2}\right)\right]^2, \tag{46}$$

for the critical value of D at which the nth peak passes through its maximum. For the deterministic firing regime ($s<1$), one can write this expression in the elegant form

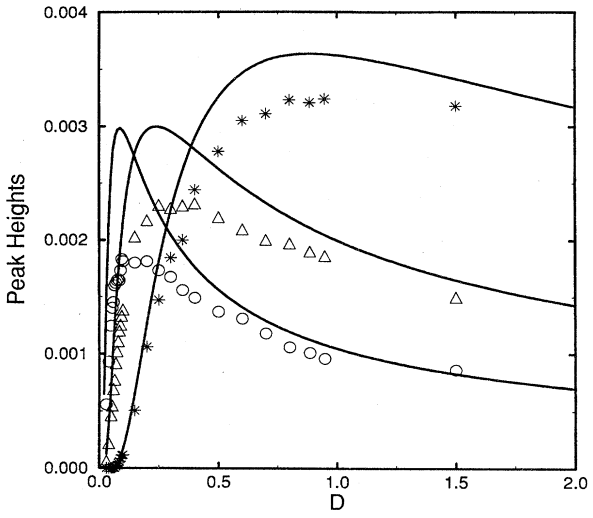

FIG. 8. Peak heights [computed from images result (16)] vs noise strength D for $n=1,2,3$ (reading right to left). Data points correspond to results obtained via direct simulation of (1): $n=1$ (asterisks), 2 (triangles), and 3 (circles). $a=20$, $\mu=0.1$, $\lambda=0.006$, $A=0.01$, $\omega=0.05$.

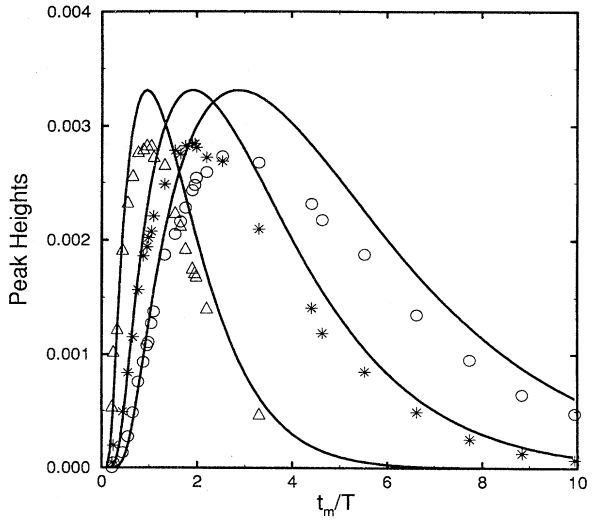

FIG. 9. Peak heights [computed from images result (16)] vs ratio t_m/T for $n=1,2,3$ (reading left to right). Data points correspond to results obtained via direct simulation of (1): $n=1$ (triangles), 2 (asterisks), and 3 (circles). $a=20$, $\mu=0.1$, $\lambda=0.006$, $A=0.01$.

$$D_{nc}\approx\frac{\mu^2/\lambda}{1-e^{-2n\lambda T}}\left[e^{-n\lambda T}-e^{-\lambda t_{a0}}\right]^2, \tag{47}$$

where Eq. (3) has been used. Clearly, the height of the nth peak, in the deterministic firing regime, increases as nT approaches the deterministic crossing time (in the absence of the modulation) t_{a0}; at the same time, the critical value of the noise strength approaches zero. In the (singular) $D\to 0$ limit, the nth peak becomes a δ function, attaining its maximum height. This behavior is completely analogous to behavior observed in the $\lambda=0$ case [12]. The arguments of the exponentials in (46) and (47) represent two characteristic time scales and the sharpness of the resonance in the height of a particular peak increases as these time scales approach each other. As we go to higher peaks, the quantitative agreement with the simulated data points worsens. However, the simulations predict a "resonance" in the peak heights, at the same critical noise strength as the method of images. In all cases, the curves produced from the method of images follow the data points more closely at increasing noise strength, reflecting our earlier observations that the method of images yields better agreement with the exact dynamics as the noise strength is increased.

Of greater interest, perhaps, is the effect of varying the modulation frequency ω. Figure 9 shows the heights of the first three peaks as a function of ω, for the leaky integrator model. The horizontal scale is the ratio of the mode, t_m, in the absence of the modulation, to the modulation period T. Here we also observe a "resonance" behavior. A given peak can be adjusted to be the highest peak in the distribution by either adjusting the system and noise parameters (for fixed stimulus frequency) so that the mode of the distribution in the $A=0$ case, coincides with the location of the peak in question, or by tuning the frequency of the drive:

$$t_m=nT. \tag{48}$$

This resonance, occurring both above and below the deterministic switching threshold, may be taken as the analog, for $n=1$, of stochastic resonance as it has been recently redefined [16] for bistable systems. Clearly, this is a resonance that corresponds to a synchronization of two characteristic times, one of which (the mode t_m) characterizes the system in the absence of the signal and the other (the period T) characterizes the signal. A similar resonance has been shown to occur in the $\lambda=0$ case [12]. Results analogous to Fig. 9 are obtained for the linear ramp model. However, for the small A values used in this work, the numerical simulations are tedious to carry out; accordingly, we do not show these results.

Below the deterministic switching threshold, a given peak can be increased still further (by decreasing the noise or increasing the drift) at the expense of the other peaks until, in the singular limit $t_m=nT\to t_0$, the nth peak becomes δ-function-like. Similar behavior has been observed and quantified in the $\lambda=0$ case [12]. Once again we observe very good qualitative agreement, insofar as the location of the resonance is concerned, with direct numerical simulations of (1). The foregoing results may be expressed in a somewhat "unified" form by plotting individual peak heights as a function of noise strength, for given frequencies ω. Figure 10 shows such a plot, computed from the images approximation (16) for the $n=2$ peak. Three different frequencies are considered. For each frequency, the second peak passes through a maximum at a critical value of the noise. The effect of the noise is to change the $A=0$ distribution moving its peak until, at the critical value of D, the second peak in the $A>0$ distribution coincides with the mode of the $A=0$ distribution. Similar behavior is seen for the remaining peaks. The critical noise parameter (at which a given peak attains its maximum

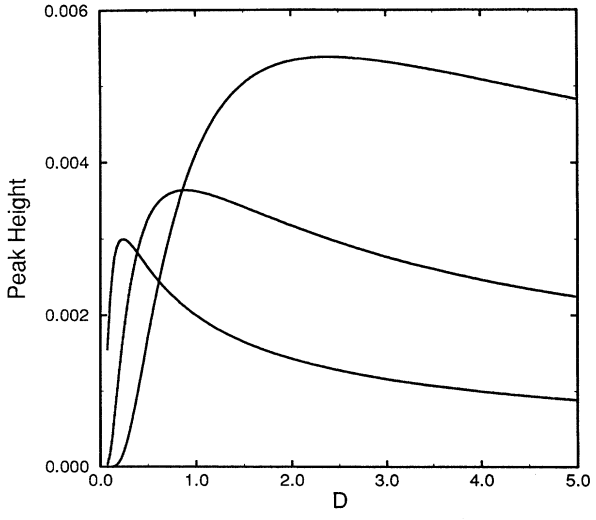

FIG. 10. Peak height ($n=2$) computed via images result (16), in the noise-activated regime as a function of noise strength D. Curves correspond to frequency $\omega=0.2$ (top), 0.1 (middle), and 0.05 (bottom). $a=20$, $\mu=0.1$, $\lambda=0.006$, $A=0.01$. Suprathreshold case, $S=1.2$.

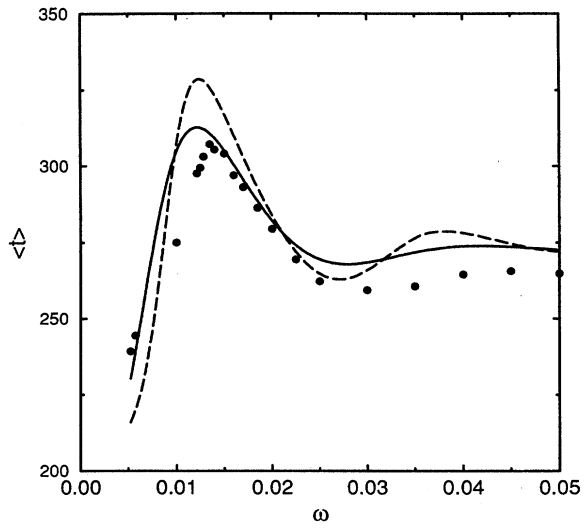

FIG. 11. Mean first passage time $\langle t\rangle$ vs stimulus frequency ω. Solid curve: $D=0.025$, dashed curve: $D=0.01$, both computed via images result (16). Data points: $\langle t\rangle$ obtained via numerical simulations of (1) with $D=0.025$. $a=20$, $\mu=0.145$, $\lambda=0.005\,75$, $A=0.025$. Subthreshold case, $S=0.79$.

height) shifts to lower values for increasing n, reflecting the fact that with increasing noise strength (keeping the drift fixed), an increasing proportion of the crossing events occur within a single cycle of the modulating signal. With decreasing D, crossing events may take more than one cycle of the modulation to occur; hence the distribution develops peaks at multiples $n>1$ of the driving period, with the mode moving toward larger values. Completely analogous behavior is observed in the deterministic firing regime.

Finally we address the issue of the mean first passage time $\langle t\rangle$ for the $A>0$ case. For the models at hand, this quantity depends on the signal frequency. Clearly, for given system and noise parameters there should be a critical value of the signal frequency at which $\langle t\rangle$ is optimized. A resonance effect does indeed occur and is shown in Figs. 11 and 12 for two system configurations corresponding, respectively, to deterministic firing and noise-activated firing. In Fig. 11 we plot the mean first passage time, computed via numerical integration using the images result (16), as a function of the applied signal frequency, in the deterministic firing regime. We note that $\langle t\rangle$ possesses (for the range of parameters considered in this work) at least one global maximum and other local maxima or minima, depending on the system and noise parameters. In the regime of this figure, the drift dominates the dynamics with the potential curvature being of minimal importance. In the $\omega\to 0$ limit, the mean first passage time converges to the deterministic passage time corresponding to an effective (constant) drift of $\mu+A$ in (1); in the opposite limit, the mean first passage time approaches the value corresponding to the $A=0$ case. As we decrease λ (or increase μ) further, this passage time becomes independent of noise, approaching the value a/μ, as discussed earlier. The data points have been obtained via numerical simulations of (1) for the $D=0.025$ case; they reproduce the important qualitative features (including the location of the resonance) of the solid curve reasonably well. Above the deterministic threshold (Fig. 12), the decay constant λ becomes increasingly important and the global maximum in $\langle t\rangle$ moves to the lower frequencies. The intercepts on the vertical axis are now separated, reflecting the fact that in this regime, the mean firing time is strongly noise-dependent. We note that varying μ and λ while keeping the ratio S fixed does not alter the behavior of the normalized mean first passage time; for the unnormalized mean first passage time this will lead only to a

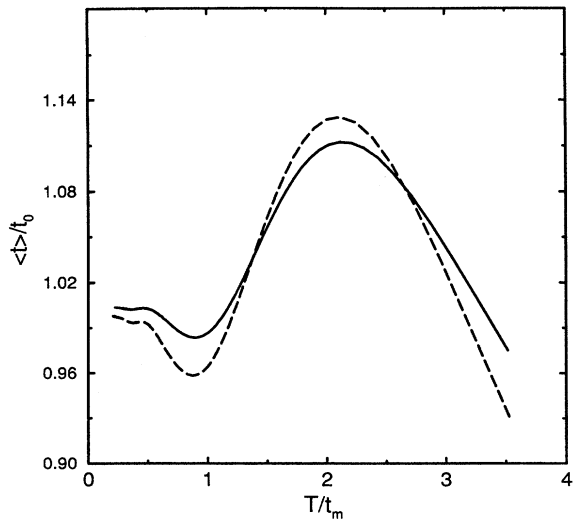

FIG. 12. Mean first passage time $\langle t\rangle$ normalized to its $A=0$ value t_0, vs T/t_m. Solid curve: $D=0.025$, dashed curve: $D=0.01$, both computed via images result (16). Same parameters as Fig. 10 except $\mu=0.1$. Suprathreshold case, $S=1.15$.

shift in the vertical axis, a quantitative change. In Fig. 12, the resonance in the mean first passage time has been represented in terms of the scaled variables $\langle t\rangle/t_0$ and T/t_m, to illustrate a point: for the weak signal amplitudes considered in this work, the magnitude of the mean first passage time is not appreciably changed by the modulating signal. We observe that the ratio $\langle t\rangle/t_0$ does not deviate substantially from unity for the weak signal amplitudes considered in this work (this is true even in the subthreshold regime) indicating that the resonances in $\langle t\rangle$ are weak but they *do* occur. In both Fig. 11 and 12, decreasing the noise strength is seen to lead to a sharper resonance; however, changing the noise strength does not appreciably shift the location of the resonance.

Before concluding, it is important to point out that the results in this paper have been derived under the assumption that the neuronal dynamics are phase-locked to the external stimulus. Mathematically, this implies that after each firing event, the refractory interval includes a waiting time until the phase of the stimulus matches the phase of the solution $x(t)$. For a phase difference different from zero, one would observe a corresponding offset in the locations of the peaks in the first passage density and quantitative changes in some of the resonance behavior described in this work; these observations have been verified numerically. In the Poisson limit of very long mean first passage time (i.e., $t_0 \gg \lambda^{-1}$) the phase decreases in importance. Also, for high driving frequencies ω, one typically passes through many cycles of the stimulus before a crossing event and a time-averaged description of the dynamics could be invoked. In the absence of a phase-locking assumption, the first passage density function displays the same general features as the densities shown in Fig. 4–7 with the important difference that the peak heights are substantially reduced (for a fixed value of the signal amplitude A).

The resonance behavior described in this section can be shown to be robust even in the absence of the phase-locking assumption. This is seen in Fig. 13 in which we plot the mean first passage time $\langle t\rangle$ computed via the method of images as well as by direct simulation of (1) with and without the phase reset. In this plot we deliberately use a high value ($A=0.085$) of the signal amplitude, corresponding to a regime in which the method of images would not be expected to yield accurate results. It is interesting that, except at very low frequencies, the simulation results are very close. This should be expected since, if we allowed the phase to remain coherent across the reset times, there would be, after an initial transient, a preferred phase at which most of the threshold crossings occurred. Figure 13 also demonstrates that the images technique yields a very good approximation to the qualitative behavior, in this case the *locations* of the resonances) of $\langle t\rangle$, even when the conditions for its validity have been substantially violated. It is clear, however, that in order to generalize the theoretical results of this work to the case of an arbitrary phase offset, one should compute a phase averaged first passage density, using a sharply peaked phase distribution function. This will be the subject of a future article.

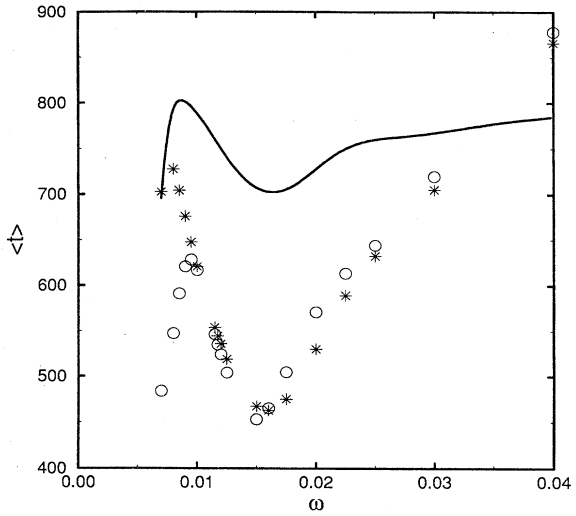

FIG. 13. Mean first passage time $\langle t\rangle$ vs frequency ω for $a=20$, $\mu=0.1$, $\lambda=0.005\,75$, $D=0.01$, $A=0.085$. Solid curve: $\langle t\rangle$ computed via images approximation (16). Data points: $\langle t\rangle$ computed via numerical simulations of (1) with phase reset (asterisks) and no phase reset (circles).

VI. CONCLUSION

The current work illustrates an important feature of neuronal firing dynamics governed by simple integrate-fire models: the noise-assisted (or mediated) synchronization to an external periodic stimulus. The method of images as well as the linear ramp model permit one to capture the important behavior of the dynamics, even in parameter regimes which deviate slightly from their regimes of validity; in particular, the *locations* of the resonances in the peak heights and the mean first passage time are correctly given by the approximations. This enables us to make the connection between the cooperative behavior observed in the first passage density function and the mean first passage time, and the stochastic resonance phenomenon that has already been quantified as a true resonance in nonlinear dynamic systems [16], as well as in simple threshold models of neurons [12]. It is apparent, in fact, that the state (characterized by the characteristic times t_m, t_0 which are functions of the drift, noise, barrier location, and decay rate) in the *absence* of the signal determines the nature of the cooperative behavior when the signal is present. In real neurons, most of the system parameters are internally adjusted and it is therefore tantalizing to conjecture that the above-described resonances might actually be a frequency selection mechanism: by adjusting these internal parameters, the response at a given multiple of an incident frequency is optimized.

ACKNOWLEDGMENTS

It is a pleasure to acknowledge useful discussions with A. Zador (Salk Inst.), L. Ricciardi (Napoli), P. Lansky (Prague), H. Tuckwell (Canberra), and F. Marchesoni and L. Gammaitoni (Perugia). A.R.B. gratefully acknowledges support from the Office of Naval Research (Physics Division) and NATO Grant No. 931464, C.R.D. acknowledges partial support from the National Science Foundation, and K.L. acknowledges partial support from the U.S. Department of Energy under Grant No. DE-FG03-86ER13606.

[1] *Proceedings of the NATO Advanced Research Workshop on Stochastic Resonance in Physics and Biology*, edited by F. Moss, A. Bulsara, and M. Shlesinger [J. Stat. Phys. **70** (1993)]; *Proceedings of the international workshop on Fluctuations in Physics and Biology: Stochastic Resonance, Signal Processing, and Related Phenomena* [Nuovo Cimento **17D** (1995)]; F. Moss, in *An Introduction to Some Contemporary Problems in Statistical Physical Physics*, edited by G. Weiss (SIAM, Philadelphia, 1994). P. Jung, Phys. Rep. **234**, 175 (1994); K. Wiesenfeld and F. Moss, Nature **373**, 33 (1995).

[2] C. R. Doering and J. C. Gadoua, Phys. Rev. Lett. **69**, 2318 (1992); J. Maddox, Nature **359**, 771 (1992); U. Zurcher and C. R. Doering, Phys. Rev. E **47**, 3862 (1992); C. Van den Broeck, *ibid.* **47**, 4579 (1992); M. Bier and R. D. Astumian, Phys. Rev. Lett. **71**, 1649 (1993); P. Hanggi, Chem. Phys. **180**, 157 (1994); P. Riemann, Phys. Rev. E **49**, 4938 (1994); P. Pechukas and P. Hanggi, Phys. Rev. Lett. **73**, 2772 (1994); L. Gammaitoni, F. Marchesoni, E. Manichella-Saetta, and S. Santucci, Phys. Rev. E **49**, 4878 (1994); J. J. Brey and J. Casado-Pascual, *ibid.* **50**, 116 (1994); P. Rieman, Phys Rev. Lett. **74**, 4576 (1995).

[3] A. Longtin, A. Bulsara, and F. Moss, Phys. Rev. Lett. **67**, 656 (1991) [see also Nature **352**, 469 (1991)]; A. Bulsara and F. Moss, in *Proceedings of the Meeting on Noise in Physical Systems and 1/f* Fluctuations ICNF91, edited by T. Musha, S. Sato, and Y. Yamamoto (Omsha, Tokyo, 1991); A. Longtin, A. Bulsara, and F. Moss, Mod. Phys. Lett. **B6**, 1299 (1992); A. Longtin, Center Nonlin. Stud. Newsl. **74** (1992) [Los Alamos Natl. Lab. Report No. LA-UR-92-163]; J. Stat. Phys. **70**, 309 (1993); K. Wiesenfeld, D. Pierson, E. Pantazelou, C. Dames, and F. Moss, Phys. Rev. Lett. **72**, 2125 (1993); A. Longtin, A. Bulsara, D. Pierson, and F. Moss, Biol. Cyb. **70**, 569 (1994); M. Riani and E. Simonotto, Phys. Rev. Lett. **72**, 3120 (1994); J. Collins, C. Chow, and T. Imhoff, Phys. Rev. E **52**, R3321 (1995).

[4] J. Douglass, L. Wilkens, E. Pantezelou, and F. Moss, Nature **365**, 337 (1993); D. Chialvo and A. Apkarian, J. Stat. Phys. **70**, 375 (1993); H. Braun, H. Wissing, K. Schafer, and M. Hirsch, Nature **367**, 270 (1994); S. Bezrukov and I. Vodyanoy, *ibid.* **378**, 362 (1995); J. Levin and J. Miller, *ibid.* **380**, 165 (1996).

[5] See, e.g., E. Montroll, in *Proceedings of Symposia in Applied Mathematics* (American Mathematics Society, Providence, RI, 1964), Vol. 26; E. Montroll and M. Shlesinger, in *Studies in Statistical Mechanics*, edited by E. Montroll and J. Lebowitz (North Holland, Amsterdam, 1984), Vol. II, and references therein.

[6] A. Siegert, Phys. Rev. **81**, 617 (1951); D. Darling and A. Siegert; Ann. Math. Stat. **24**, 624 (1953).

[7] A. Bharucha-Reid, *Elements of the Theory of Markov Processes and their Applications* (McGraw-Hill, New York, 1960); D. Cox and H. Miller, *The Theory of Stochastic Processes* (Chapman and Hall, London, 1965); W. Feller, *An Introduction to Probability Theory and its Applications* (Wiley, New York, 1971), Vol. 2; I. Blake and W. Lindsey, IEEE Trans. Inf. Theory **IT-19**, 295 (1973).

[8] G. Uhlenbeck and L. Ornstein, Phys. Rev. **36**, 823 (1930); S. Chandrasekhar, Rev. Mod. Phys. **15**, 1 (1943); M. Wang and G. Uhlenbeck, *ibid.* **17**, 323 (1945); M. Kac, in *Selected Papers on Noise and Stochastic Processes*, edited by N. Wax (Dover, New York, 1954).

[9] L. Ricciardi, *Diffusion Processes and Related Topics in Biology* (Springer-Verlag, Berlin, 1977); H. Tuckwell, *Stochastic Processes in the Neurosciences* (SIAM, Philadelphia, 1979); *Introduction to Theoretical Neurobiology* (Cambridge University Press, Cambridge, 1988).

[10] L. Abbott and T. Kepler, in *Statistical Mechanics of Neural Networks*, edited by L. Garrido (Springer-Verlag, Berlin 1990).

[11] G. Gerstein and B. Mandelbrot, Biophys. J. **4**, 41 (1964).

[12] A. Bulsara, S. Lowen, and C. Rees, Phys. Rev. E **49**, 4989 (1994).

[13] P. Lansky, Ph.D. thesis, Prague, 1982.

[14] H. Tuckwell and F. Wan, J. Appl. Prob. **21**, 695 (1984); E. Fletcher, S. Havlin, and G. Weiss, J. Stat. Phys. **51**, 215 (1988); V. Giorno, A. Nobile, and L. Ricciardi, Adv. Appl. Prob. **22**, 883 (1990).

[15] K. Lindenberg, K. Shuler, J. Freeman, and T. Lie, J. Stat. Phys. **12**, 217 (1975).

[16] L. Gammaitoni, F. Marchesoni, and S. Santucci, Phys. Rev. Lett. **74**, 1052 (1995).

[17] F. Chapeau-Blondeau, X. Godivier, and N. Chambet, Phys. Rev. E **53**, 1276 (1996).

[18] See, e.g., C. Gardiner, *Handbook of Stochastic Processes* (Springer-Verlag, Berlin 1983); H. Risken, *The Fokker Planck Equation* (Springer-Verlag, Berlin, 1984).

[19] See, e.g., H. Sugiyama, G. Moore, and D. Perkel; Math. Biosci. **8**, 323 (1970); C. Ascoli, C. Frediani, and D. Petracchi, in *Progress in Cybernetics and Systems Research*, edited by R. Trappl, L. Ricciardi, and G. Pask (McGraw-Hill, New York, 1982), Vol. 9.